SIAM J. Imaging Sciences
Vol. 3, No. 3, pp. 646–669

Learning the Morphological Diversity*

Gabriel Peyré[†], Jalal Fadili[‡], and Jean-Luc Starck[§]

Abstract. This article proposes a new method for image separation into a linear combination of morphological components. Sparsity in fixed dictionaries is used to extract the cartoon and oscillating content of the image. Complicated texture patterns are extracted by learning adapted local dictionaries that sparsify patches in the image. These fixed and learned sparsity priors define a nonconvex energy, and the separation is obtained as a stationary point of this energy. This variational optimization is extended to solve more general inverse problems such as inpainting. A new adaptive morphological component analysis algorithm is derived to find a stationary point of the energy. Using adapted dictionaries learned from data allows one to circumvent some difficulties faced by fixed dictionaries. Numerical results demonstrate that this adaptivity is indeed crucial in capturing complex texture patterns.

Key words. adaptive morphological component analysis, sparsity, image separation, inpainting, dictionary learning, cartoon images, texture, wavelets

AMS subject classifications. 41A25, 42C40, 65T60

DOI. 10.1137/090770783

Introduction. Morphological diversity is a concept in which an image is modeled as a sum of components, each of these components having a given morphological signature. Sparsity in a redundant dictionary can be used to discriminate between these signatures, and fast algorithms such as the morphological component analysis (MCA) have been developed in order to reconstruct simultaneously all of the morphological components [54]. For natural images containing edges and contours, two fixed dictionaries can be used, such as the local discrete cosine transform (DCT) for sparsely representing the texture and the curvelet for the edges [55]. Results were interesting, but this approach bears some limitations since complicated textures may not be well represented by the local DCT, leading to a bad separation.

This paper extends the morphological diversity by learning the morphologies of complicated texture layers to help the separation process. These learned dictionaries are coupled with more traditional fixed morphologies to characterize the cartoon and oscillating content of an image. A new adaptive morphological component analysis algorithm performs iteratively both the learning and the separation.

[*] Received by the editors September 11, 2009; accepted for publication (in revised form) June 25, 2010; published electronically September 29, 2010.
http://www.siam.org/journals/siims/3-3/77078.html

[†] Ceremade, Université Paris-Dauphine, Place du Maréchal De Lattre De Tassigny, 75775 Paris Cedex 16, France (gabriel.peyre@ceremade.dauphine.fr).

[‡] GREYC CNRS-ENSICAEN-Université de Caen 6, Bd du Maréchal Juin, 14050 Caen Cedex, France (jalal.fadili@greyc.ensicaen.fr).

[§] Service d'Astrophysique, CEA/Saclay, Orme des Merisiers, Bat 709, 91191 Gif-sur-Yvette Cedex, France (jstarck@cea.fr).

1. Image separation and inverse problem regularization.

1.1. Image separation.

The image separation process decomposes an input image $u \in \mathbb{R}^N$ of N pixels into a linear combination of $|\Lambda|$ layers $\{u_s\}_{s\in\Lambda}$, the so-called morphological components

$$u = \sum_{s\in\Lambda} u_s + \varepsilon, \tag{1.1}$$

where ε is an error term representing the noise and model imperfections. Each u_s accounts for a different kind of feature of the original data u.

Image separation is usually achieved by solving a variational optimization problem of the form

$$\min_{\{u_s\}_{s\in\Lambda}} \frac{1}{2}\Big\| u - \sum_{s\in\Lambda} u_s \Big\|^2 + \mu \sum_{s\in\Lambda} E_s(u_s), \tag{1.2}$$

where each energy $E_s : \mathbb{R}^N \mapsto \mathbb{R}^+$ favors images with some specific kind of structure. More precisely, for successful separation, each energy E_s is designed to be as small as possible over the layer u_s it is serving, while being large (or at least not as small) over the other components. Thus each of these layers has its attached prior E_s, and multiplying the number of priors might help to recover intricate image structures such as smooth areas, edges, and textures of natural images.

1.2. Inverse problems regularization.

Many problems in image processing can be cast as inverting a linear system $f = \mathcal{K}u + \varepsilon$, where $u \in \mathbb{R}^N$ is the data to recover, $f \in \mathbb{R}^m$ is the observed image, and ε is a Gaussian white noise of known finite variance. The bounded linear operator $\mathcal{K} : \mathbb{R}^N \mapsto \mathbb{R}^m$ is typically ill-behaved since it models an acquisition process that entails loss of information. This yields ill-posedness of the inverse problem.

This inversion problem is regularized by adding some prior knowledge of the typical structures of the original image u. This prior information accounts for the smoothness of the solution and can range from uniform smoothness assumption to more complex knowledge of the geometrical structures of u. The decomposition problem (1.2) is extended to handle an ill-behaved operator $\mathcal{K}$ which yields the following minimization problem:

$$\min_{\{u_s\}_{s\in\Lambda}} \frac{1}{2}\Big\| f - \mathcal{K}\sum_{s\in\Lambda} u_s \Big\|^2 + \mu \sum_{s\in\Lambda} E_s(u_s)\ . \tag{1.3}$$

The simple case of image separation (1.1) corresponds to $\mathcal{K} = \mathrm{Id}_N$. Typical examples of inverse problems include deconvolution, inpainting, and superresolution. In the latter, one seeks to recover a high-resolution image u from a low-resolution observation f. In such a case, $\mathcal{K}$ is the convolution by a blurring kernel followed by a subsampling, and f lacks the high frequency content of u.

There is a flurry of research activity on linear inverse problem regularization in image processing. Comprehensive overviews can be found in dedicated monographs.

Sparsity-based regularization (e.g., in the wavelet domain) methods have recently received considerable attention, either by adopting a Bayesian expectation-maximization framework

[26, 27, 6], by introducing surrogate functionals [14], or by using a proximal forward-backward splitting framework [12, 25]. This framework has been successfully applied to inpainting [22, 25], deconvolution [24], multichannel data restoration, and blind source separation [61, 7].

1.3. Image inpainting.

This paper considers the inpainting inverse problem, although our method applies to other linear inverse problems as well. Inpainting is to restore missing image information based upon the still available (observed) cues from destroyed or deliberately masked subregions of the image f.

The inpainting problem corresponds to a diagonal operator

$$\mathcal{K} = \operatorname{diag}_i(\eta_i), \qquad \text{where} \qquad \eta_i = \begin{cases} 1 & \text{if} \quad i \notin \Omega, \\ 0 & \text{if} \quad i \in \Omega, \end{cases}$$

where $\Omega \subset \{0, \dots, N-1\}$ denotes the set of missing pixels.

Inpainting of nontextured images has traditionally been approached by diffusion equations that progressively fill the missing pixels. The original work of Masnou makes use of the continuation law of the level sets [40]. Following their work, several authors proposed high order PDEs (see, for instance, [10, 5, 3]) and anisotropic diffusion [57] for nontexture inpainting. The inpainting of complicated textures can be achieved by using copy-and-paste methods from computer graphics [19, 13] and can successfully inpaint large missing regions. MCA is able to solve the inpainting problem [22, 25] for images containing simple textural content such as locally parallel oscillations. Methods based on learning sparse dictionaries [36, 33] and training fields of experts [51] are able to inpaint small missing regions.

2. Morphological diversity modeling with sparsity.

2.1. Cartoon modeling.

For the sketchy part of an image, a usual prior is to assume that it belongs to some nonlinear Banach space that favors the discontinuities in the image. In particular, this entails that the functional norm of the sketchy part in such spaces is small. Such spaces include the bounded variation (BV) space with the associated total variation norm introduced by Rudin, Osher, and Fatemi [52]. Another important prior exploits smoothness in Besov spaces for which the wavelet transform is known to provide a sparse respresentation. A standard example of such a sparsity-promoting prior is the ℓ^1-norm introduced by Donoho and Johnstone [17] in the wavelet context for denoising purposes.

Wavelets are, however, suboptimal in efficiently capturing edge singularities distributed along smooth curves. The curvelet tight frame, introduced by Candès and Donoho [9], is able to better represent cartoon images with smooth edges. Sparsity in a curvelet tight frame can thus improve the modeling of edges.

2.2. Oscillating texture modeling.

Simple texture models can also be defined through variational energies that favor oscillations in images. Toward this goal, Meyer introduced a functional space where oscillating patterns have a small norm. It turns out that this Banach space is close to the dual of the BV space [42]. Meyer defined the so-called G-norm that can be used to perform the decomposition of an image into a cartoon component (using, for instance, the total variation seminorm) and an oscillating texture component.

The work of Meyer paved the way for an active research area in variational image processing: cartoon+texture image decomposition. Several authors have proposed algorithms to solve Meyer's problem or close extensions, such as [60, 2, 32] to cite only a few.

Sparsity-based energies have also been proposed for decomposing an image into cartoon+ oscillating texture. To this end, Starck and coauthors [55, 54, 22] introduced the MCA framework, where overcomplete fixed dictionaries (one for each layer) are used as a source of diversity to discriminate between the components. The key is that each dictionary must sparsify the corresponding layer while being highly inefficient in representing the other content. For example, MCA is capable of decomposing an image into structure+oscillating texture, using the wavelet or curvelet dictionary for the cartoon layer, and the frame of local cosines for the oscillating texture.

Other dictionaries can enhance the results of local cosines to capture warped locally oscillatory patterns. For instance, the waveatoms of Demanet and Ying [15] and the brushlets of Meyer and Coifman [41] have been designed for this goal.

However, the standard MCA is intrinsically limited by the discriminative performance of its fixed nonadaptive dictionaries. Obviously, the latter are not able to sparsify complex textures appearing in natural images.

2.3. Adaptivity and dictionary learning.

To enhance the modeling of complicated edge layouts and intricate texture patterns, one needs to resort to adapted energies, which are tuned to fit the geometry of complex images.

A class of adaptive methods consists in using a family of orthogonal bases and looking for the best basis in this family using combinatorial optimization algorithms. The wedgelets [16] and the bandlets [29, 39] better represent contours than a traditional wavelet dictionary. For oscillating textures, a proper basis of the wavelet packet tree [37] with an appropriate tiling of the frequency domain sparsifies some oscillatory patterns. Cosine packets allow a dyadic partition of the spatial domain [37] according to a quad-tree structure. Grouplet bases [38] are able to approximate efficiently oscillating and turbulent textures and were successfully applied to texture synthesis and inpainting in [48].

In contrast to these approaches, which are able to handle only a particular kind of image or texture, other approaches can adapt to the content of images through a learning process. By minimizing a sparsity criterion, such algorithms allow one to optimize a local dictionary for a set of exemplar patches.

Olshausen and Field [45] were the first to propose a way of learning the dictionary from the data and to insist on the dictionary redundancy. They have applied this learning scheme to patches extracted from natural images. The major conclusion of this line of research is that learning over a large set of disparate natural images leads to localized oriented edge filters. Since then, other approaches to sparse coding have been proposed using independent component analysis [4] or different sparsity priors on the representation coefficients [31, 28, 23, 1].

It is worth pointing out that this dictionary learning bears close similarities to sparsity-based blind source separation (BSS) algorithms as proposed in [61] and in the generalized morphological component analysis (GMCA) algorithm [7]. It is also related to nonnegative matrix factorization that is used for source separation; see, for instance, [47]. The role played by the dictionary parallels that of the mixing matrix in BSS.

These learned dictionaries have proved useful in performing image denoising [20], inpainting [36, 33], texture synthesis [49], and image recognition [35].

A preliminary description of the adaptive MCA method was presented in [50]. Shoham and Elad developed in [53] an adaptive separation method that approximately minimizes our adaptive MCA energy. This method is faster if no global dictionary is used.

2.4. Contributions. This paper proposes a new adaptive image separation method. It extends previous work on MCA by adapting the dictionary used to model and discriminate complex texture layer(s). Section 3 introduces the notions of fixed and learned dictionaries, which can be combined to achieve high quality separation. The local dictionaries are learned during the separation within a new adaptive MCA algorithm detailed in section 4. This algorithm converges to a stationary point of a nonconvex variational energy. Numerical results show that a single adaptive texture layer can be trained without user intervention to extract a complicated texture. Additional layers can be added as well, and in this case, a proper user-defined initialization is required to drive the algorithm to the desired decomposition which corresponds to a particular stationary point of the energy. This option offers some flexibility to the user in guiding the decomposition algorithm toward the desired solution.

3. Fixed and adaptive sparsity energies.

Each energy $E_s(u_s)$ depends on a dictionary D_s that is a collection of atoms used to sparsely describe the component u_s. This paper considers both fixed dictionaries, which are used to describe the content of the component as a whole, and local learned dictionaries, which are applied to patches extracted from the component.

The set of indexes is thus decomposed as $\Lambda = \Lambda^{\mathrm{F}} \cup \Lambda^{\mathrm{L}}$, and a fixed layer $s \in \Lambda^{\mathrm{F}}$ is assigned an energy $E^{\mathrm{F}}(u_s, D_s)$, whereas an energy $E^{\mathrm{L}}(u_s, D_s)$ is attached to a layer $s \in \Lambda^{\mathrm{L}}$ with a learned dictionary. The fixed dictionaries are defined by the user and correspond typically to a cartoon morphological component or simple oscillating patterns. On the contrary, learned dictionaries $\{D_s\}_{s\in\Lambda^{\mathrm{L}}}$ are optimized by our algorithm to capture complicated stationary texture patterns. The corresponding adaptive separation process thus extends (1.2) to an optimization on both the components and the adaptive dictionaries:

$$(3.1) \qquad \min_{\{u_s\}_{s\in\Lambda}, \{D_s \in \mathcal{D}_s\}_{s\in\Lambda^{\mathrm{L}}}} \frac{1}{2}\Big\| f - \mathcal{K}\sum_{s\in\Lambda} u_s \Big\|^2 + \mu \sum_{s\in\Lambda^{\mathrm{F}}} E^{\mathrm{F}}(u_s, D_s) + \mu \sum_{s\in\Lambda^{\mathrm{L}}} E^{\mathrm{L}}(u_s, D_s),$$

where $\mathcal{D}_s$ is a suitable set of convex constraints to be defined later (see (4.3)).

3.1. Sparsity-based energy for a fixed dictionary.

A fixed dictionary $D_s = (d_{s,j})_{0\leqslant j<m_s}$, for $s \in \Lambda^{\mathrm{F}}$, is a (possibly redundant) collection of $m_s \geqslant N$ atoms $d_{s,j} \in \mathbb{R}^N$, which can be represented as a rectangular matrix $D_s \in \mathbb{R}^{N\times m_s}$. The decomposition of a component u_s using this dictionary reads as

$$u_s = D_s x_s = \sum_{j=0}^{m_s-1} x_s[j] d_{s,j}.$$

For a redundant dictionary where $m_s > N$, such a decomposition is nonunique, and a sparsity-promoting energy favors sparse coefficients x_s, for which most of the entries $x_s[j]$ are zero. In this paper, we use a convex ℓ^1 sparsity measure

$$\|x_s\|_1 = \sum_j |x_s[j]|,$$

which was proposed by Chen, Donoho, and Saunders [11] in the popular basis pursuit denoising problem (BPDN or Lasso for statisticians) for sparse approximation.

Finding a sparse approximation $D_s x_s$ of u_s in D_s can then be formulated as minimizing the energy

$$E^{\mathrm{F}}(u_s, D_s) = \min_{x_s \in \mathbb{R}^{m_s}} \mathcal{E}^{\mathrm{F}}(u_s, x_s, D_s), \tag{3.2}$$

$$\text{where} \quad \mathcal{E}^{\mathrm{F}}(u_s, x_s, D_s) = \frac{1}{2}\|u_s - D_s x_s\|^2 + \lambda \|x_s\|_1. \tag{3.3}$$

The parameter λ allows an approximate sparse representation $D_s x_s \approx u_s$ and should be adapted to the level of the noise and the sparsity of the sources.

Cartoon sparse models. Wavelets [37] are used extensively in image compression and allow one to efficiently capture images with isotropic singularities and images with bounded variation. We use a redundant dictionary D_{wav} of translation invariant wavelets to capture the sketchy content of an image, which is assumed to have a small total variation.

To capture more regular edge patterns, we use a redundant tight frame of curvelets D_{curv}, introduced by Candès and Donoho [9] to optimally represent cartoon images with C^2-regular edge curves.

Oscillating sparse models. Locally oscillating and stationary textures are handled with a redundant tight frame D_{dct} of local cosines [37]. We use local cosine atoms defined on blocks of 32×32 pixels, which are zero outside the blocks and are thus vectors of length N. We use an overlapping factor of 2 of the blocks along the horizontal and vertical directions, so that the redundancy of D_{dct} is $m_s/N = 4$. As explained in the introduction, other dictionaries well suited for sparsifying oscillating patterns could be used as well, e.g., waveatoms [15].

3.2. Sparsity-based energy for a learned dictionary.

We use local learned dictionaries $\{D_s\}_{s \in \Lambda^{\mathrm{L}}}$ to capture fine scale structures of complex textures. For $s \in \Lambda^{\mathrm{L}}$, a local learned dictionary $D_s \in \mathbb{R}^{n \times m_s}$ is used to represent patches $R_k(u_s) \in \mathbb{R}^n$ of $n = \tau \times \tau$ pixels extracted from a component u_s:

$$\forall\, 0 \leqslant k_{1,2} < \sqrt{N}/\Delta \quad \text{and} \quad -\tau/2 \leqslant i_{1,2} < \tau/2, \quad R_k(u_s)[i] = u_s(k_1\Delta + i_1, k_2\Delta + i_2),$$

where $i = (i_1, i_2)$ is the location of a pixel in the patch, $k = (k_1, k_2)$ indexes the central location of the patch, and $1 \leqslant \Delta \leqslant \tau$ controls the subsampling of the patch extraction process. Although k is a pair of integers to index two-dimensional patches, it is conveniently converted into a single integer in $\{0, \ldots, N/\Delta^2 - 1\}$ after rearranging the patches in a vectorized form to store them as column vectors in a matrix.

Similarly to the energy (3.2) associated to a fixed dictionary, we define an energy $E^{\mathrm{L}}(u_s, D_s)$ associated to a local dictionary D_s. This energy allows one to control the sparsity of the decomposition of all of the patches $R_k(u_s)$ in D_s. Following Aharon and Elad [20] and Aharon, Elad, and Bruckstein [1], we define this energy $E^{\mathrm{L}}(u_s, D_s)$ as

$$E^{\mathrm{L}}(u_s, D_s) = \min_{\{x_{s,k}\}_k \in \mathbb{R}^{m_s \times N/\Delta^2}} \mathcal{E}^{\mathrm{L}}(u_s, \{x_{s,k}\}_k, D_s), \tag{3.4}$$

$$\text{where} \quad \mathcal{E}^{\mathrm{L}}(u_s, \{x_{s,k}\}_k, D_s) = \frac{1}{p} \sum_k \left(\frac{1}{2} \|R_k(u_s) - D_s x_{s,k}\|^2 + \lambda \|x_{s,k}\|_1 \right), \tag{3.5}$$

where $p = (\tau/\Delta)^2 = n/\Delta^2$. Each $x_{s,k}$ corresponds to the coefficients of the decomposition of the patch $R_k(u_s)$ in the dictionary D_s. The weight $1/p$ in the energy (3.4) compensates for the redundancy factor introduced by the overlap between the patches $\{R_k(u_s)\}_k$. This normalization allows one to rescale the learned dictionary energy (3.4) to be comparable with the fixed dictionary energy (3.2).

3.3. Images vs. coefficients.

The variational formulation (1.3) proposed in this paper directly seeks the components $\{u_s\}_{s\in\Lambda}$, and the coefficients are considered only as auxiliary variables. Alternative formulations of inverse problems in redundant dictionaries or union of bases would look instead for the coefficients x_s or $\{x_{s,k}\}_k$ of each component in the dictionary D_s.

The corresponding coefficient-based minimization reads as

$$(\{x_s^\star\}_{s\in\Lambda}, \{D_s^\star\}_{s\in\Lambda^{\mathrm{L}}}) \in \underset{\{x_s\}_{s\in\Lambda}, \{D_s \in \mathcal{D}_s\}_{s\in\Lambda^{\mathrm{L}}}}{\operatorname{argmin}} \tag{3.6}$$

$$\frac{1}{2} \left\| f - \mathcal{K} \sum_{s\in\Lambda^{\mathrm{F}}} D_s x_s - \mathcal{K} \sum_{s\in\Lambda^{\mathrm{L}},k} R_k^*(D_s x_{s,k}) \right\|^2 + \lambda \sum_{s\in\Lambda^{\mathrm{F}}} \|x_s\|_1 + \lambda \sum_{s\in\Lambda^{\mathrm{L}},k} \|x_{s,k}\|_1, \tag{3.7}$$

where the dual operator R_k^* reconstructs an image in $\mathbb{R}^N$ with zero values outside the patch. Such a coefficient-based optimization is used for fixed dictionaries in [55, 22, 25].

A fixed dictionary component for $s \in \Lambda^{\mathrm{F}}$ is retrieved from these optimized coefficients as $u_s^\star = D_s x_s^\star$. For a local learned dictionary, the reconstructions of the patches are summed:

$$\forall\, s \in \Lambda^{\mathrm{L}}, \quad u_s^\star = \sum_k R_k^*(D_s^\star x_{s,k}^\star). \tag{3.8}$$

The reconstruction formula (3.8) shows that the optimization (3.7) for the learned component $s \in \Lambda^{\mathrm{L}}$ corresponds to finding a sparse approximation of u_s in the highly redundant dictionary $\{R_k^*(d_{s,j})\}_{k,j}$ that gathers all the atoms at all patch locations.

The two formulations (1.3) and (3.7) are expected to differ significantly. These differences share some similarities with the formulations analyzed in [21], which studies analysis and synthesis signal priors. In our setting, where we use local learned dictionaries, the formulation (1.3) over the image domain makes more sense. In this formulation, each patch is analyzed independently by the sparsity prior, and the ℓ^2 fidelity term linearly gathers the contributions of the patches to obtain u_s. As noted by Aharon and Elad (see [20, 1]), this average of sparse representations has some flavor of minimum mean square estimation, which helps to further reduce the noise.

Furthermore, formulation (3.7) corresponds to the optimization of coefficients in a highly redundant dictionary, which is numerically demanding. In contrast, our formulation (1.3) allows for an iterative scheme that optimizes the coefficients independently over each patch and averages them afterward. We describe this adaptive MCA scheme in the following section.

The last chief advantage of (1.3) is that it decouples the contribution of each local learned dictionary D_s for $s \in \Lambda^{\mathrm{L}}$. This simplifies the learning process, since each dictionary is independently optimized during the iterations of our adaptive MCA.

4. Adaptive morphological component analysis.

The MCA algorithm [55, 54] allows one to iteratively solve the variational separation problem (1.3) for sparsity-based energies E_s as defined in (3.2). For the decomposition of an image into its geometrical and textured parts, the original approach [55, 54] uses fixed dictionaries of wavelets D_{wav}, curvelets D_{curv}, and local cosines D_{dct}. This paper extends the MCA algorithm to deal with energies E_s associated to local learned dictionaries D_s as defined in (3.4). In addition, our adaptive MCA algorithm is able to optimize the local dictionaries D_s, which are automatically adapted to the texture to be extracted.

4.1. Adaptive variational problem.

The new adaptive MCA algorithm iteratively minimizes the energy (1.3) by adding to the decomposition variables $\{u_s\}_{s\in\Lambda}$ and $\{D_s\}_{s\in\Lambda^{\mathrm{L}}}$ auxiliary variables $\{x_s\}_{s\in\Lambda}$ corresponding to the coefficients of the decomposition of each u_s. For a fixed dictionary layer $s \in \Lambda^{\mathrm{F}}$, these coefficients are stored in a vector $x_s \in \mathbb{R}^{m_s}$. For a local learned dictionary $s \in \Lambda^{\mathrm{L}}$ these coefficients are a collection of vectors $\{x_{s,k}\}_{k=0}^{N/\Delta^2-1} \in \mathbb{R}^{m_s \times N/\Delta^2}$.

The energy minimized by the adaptive MCA algorithm is

$$\mathcal{E}(\{u_s\}_s, \{x_s\}_s, \{D_s \in \mathcal{D}_s\}_{s\in\Lambda^{\mathrm{L}}}) = \frac{1}{2}\left\| f - \mathcal{K}\sum_s u_s \right\|^2 \tag{4.1}$$

$$+ \mu \sum_{s\in\Lambda^{\mathrm{F}}} \mathcal{E}^{\mathrm{F}}(u_s, x_s, D_s) + \mu \sum_{s\in\Lambda^{\mathrm{L}}} \mathcal{E}^{\mathrm{L}}(u_s, x_s, D_s), \tag{4.2}$$

where the fixed and learned energies $\mathcal{E}^{\mathrm{F}}$ and $\mathcal{E}^{\mathrm{L}}$ are defined in (3.3) and (3.5).

The constraint $D_s = (d_{j,s})_{0\leqslant j<m_s} \in \mathcal{D}_s$ for $s \in \Lambda^{\mathrm{L}}$ ensures that the columns $d_{i,s}$ of D_s have bounded norm

$$\forall\, j = 0, \dots, m_s - 1, \quad \|d_{j,s}\|^2 = \sum_i |d_{j,s}[i]|^2 \leqslant 1.$$

This avoids the classical scale indeterminacy between the dictionaries and the coefficients since replacing (D_s, x_s) by $(aD_s, x_s/a)$ for $a > 1$ leaves the data fidelity term unchanged, while diminishing the ℓ^1 penalty. We also impose that the atoms have zero mean, which is consistent with the intuition that a texture locally contains only high frequencies. The convex set $\mathcal{D}_s$ reads as

$$\mathcal{D}_s = \left\{ D \in \mathbb{R}^{n\times m_s} \setminus \forall\, j = 0, \dots, m_s - 1,\ \|d_{j,s}\| \leqslant 1 \text{ and } \sum_i d_{j,s}[i] = 0 \right\}. \tag{4.3}$$

Additional constraints. We note that other constraints could be used to better control the stability of the learned dictionaries. For instance, an orthogonality constraint has been considered by Lesage et al. [30]. It could also be incorporated into our constraint set $\mathcal{D}_s$. Additional constraints could be considered to improve the separation. In particular, forcing the atoms of two distinct dictionaries D_s and $D_{s'}$ to have different morphologies might increase the quality of the separation. Investigation of such additional constraints is left for a future work.

Adaptive nonconvex minimization. The energy $\mathcal{E}$ is marginally convex in each of its arguments and is optimized over a convex set. However, $\mathcal{E}$ is jointly nonconvex in all of its arguments. We thus propose an iterative block relaxation coordinate descent minimization scheme and show that it converges to a stationary point of the energy.

The adaptive MCA algorithm operates by successively and cyclically minimizing $\mathcal{E}$ on the set of components $\{u_s\}_{s\in\Lambda}$, on the set of coefficients $\{x_s\}_{s\in\Lambda}$, and on the set of learned dictionaries $\{D_s\}_{s\in\Lambda^{\mathrm{L}}}$. Each minimization is performed while all remaining variables are held fixed.

The initialization of the dictionaries $\{D_s\}_{s\in\Lambda^{\mathrm{L}}}$ is thus important, and user intervention can improve the result by selecting initial features that are relevant for texture extraction.

4.2. Parameter selection.

Selecting optimal values for μ and λ is a delicate and difficult task. The parameter μ is adapted to the noise level. In the case where ε is a Gaussian white noise of variance σ, μ is set so that the residuals satisfy $\|f - \mathcal{K}\sum_s u_s^\star\| \approx \sqrt{N}\sigma$, which works well for separation and denoising applications. The same weight λ could be chosen for all dictionaries (i.e., components). Nevertheless, if additional prior knowledge of the amplitude of each component is available, it could be wisely incorporated by selecting different weights. In our experiments, we set $\lambda = \sigma^2/30$, which was shown by Aharon and Elad (see [20, 1]) to be a good choice for denoising applications.

The choice of the size of the learned dictionaries (size of the patch $n = \tau^2$ and redundancy m_s/n) is still largely an open question in dictionary learning. For inpainting, the size of the patches should be chosen larger than that of the missing regions. Increasing the redundancy of the dictionary enables one to capture more complicated textures but makes the learning more difficult both computationally (complexity increases with overcompleteness) and in terms of convergence to a poor local minimum (conditioning of the dictionary deteriorates with increasing redundancy).

4.3. Step 1: Update of the coefficients $\{x_s\}_{s\in\Lambda}$.

The update of the coefficients requires the minimization of $\mathcal{E}$ with respect to $\{x_s\}_{s\in\Lambda}$. Since this problem is separable in each of the coefficient vectors x_s, we perform the optimization independently for the coefficients of each fixed layer or each patch in a learned dictionary layer.

For a fixed dictionary $s \in \Lambda^{\mathrm{F}}$, this corresponds to solving

$$x_s \in \underset{x\in\mathbb{R}^{m_s}}{\operatorname{argmin}}\ \frac{1}{2}\|u_s - D_s x\|^2 + \lambda\|x\|_1. \tag{4.4}$$

For a learned dictionary $s \in \Lambda^{\mathrm{L}}$, the minimization is performed with respect to each patch index k:

$$x_{s,k} \in \underset{x\in\mathbb{R}^{m_s}}{\operatorname{argmin}} \frac{1}{2}\|R_k(u_s) - D_s x\|^2 + p\lambda\|x\|_1. \tag{4.5}$$

Both (4.4) and (4.5) correspond to sparse coding by minimizing a basis pursuit denoising problem [11]. The literature is inundated by a variety of algorithms trying to solve this convex problem efficiently, among which are interior point solvers [11], iterative soft thresholding [14, 12], or the Nesterov multistep scheme [43, 44].

4.4. Step 2: Update of the components $\{u_s\}_{s\in\Lambda}$.

Updating the components $\{u_s\}_{s\in\Lambda}$ requires solving a quadratic minimization problem

$$\min_{\{u_s\}_{s\in\Lambda}} \left\| f - \mathcal{K}\sum_{s\in\Lambda} u_s \right\|^2 + \mu \sum_{s\in\Lambda^{\mathrm{F}}} \|u_s - D_s x_s\|^2 + \frac{\mu}{p}\sum_{s\in\Lambda^{\mathrm{L}},k} \|R_k(u_s) - D_s x_{s,k}\|^2. \tag{4.6}$$

This is a high-dimensional problem since it involves all the layers and can be solved with a conjugate gradient descent.

An alternate method consists in cycling repeatedly on each component u_s for $s \in \Lambda$ and optimizing (4.6) with respect to u_s alone. This generates iterates $u_s^{(\ell)}$ that ultimately converge to a global minimizer of (4.6). Although the convergence is slower than with a conjugate gradient descent, it is simpler to implement since each component update is easy to compute in closed form.

At a step ℓ of this update of the components, a new iterate $u_s^{(\ell+1)}$ is obtained by minimizing (4.6) with respect to u_s alone. For a fixed dictionary $s \in \Lambda^{\mathrm{F}}$, this leads to

$$u_s^{(\ell+1)} = \underset{u\in\mathbb{R}^N}{\operatorname{argmin}} \|r_s - \mathcal{K}u\|^2 + \mu\|u - D_s x_s\|^2 \quad \text{with} \quad r_s = f - \mathcal{K}\sum_{s'\neq s} u_{s'}^{(\ell)},$$

and for a learned dictionary $s \in \Lambda^{\mathrm{L}}$ to

$$u_s^{(\ell+1)} = \underset{u\in\mathbb{R}^N}{\operatorname{argmin}} \|r_s - \mathcal{K}u\|^2 + \frac{\mu}{p}\sum_k \|R_k(u) - D_s x_{s,k}\|^2.$$

Note that we use an equality and not an inclusion since the marginal objective is strictly (in fact, strongly) convex in u; therefore it has a unique global minimizer in this coordinate.

This leads to the closed-form update rule

$$u_s^{(\ell+1)} = \left(\mathcal{K}^*\mathcal{K} + \mu\mathrm{Id}_N\right)^{-1}\left(\mathcal{K}^* r_s + \mu\hat{u}_s\right), \tag{4.7}$$

where the reconstructed $\hat{u}_s$ is computed differently depending on whether the dictionary is fixed or learned:

$$\hat{u}_s = \begin{cases} D_s x_s & \text{if} \quad s \in \Lambda^{\mathrm{F}}, \\ \dfrac{1}{p}\displaystyle\sum_k R_k^*(D_s x_{s,k}) & \text{if} \quad s \in \Lambda^{\mathrm{L}}. \end{cases} \tag{4.8}$$

To derive the expression for a learned dictionary, we used the fact that

$$\frac{1}{p}\sum_k R_k^* R_k = \mathrm{Id}_N,$$

and special care should be taken at the boundaries of the image.

For a general operator $\mathcal{K}$, the update (4.7) requires solving a well-conditioned linear system, which can be computed by conjugate gradient. If $\mathcal{K}$ is known to be diagonalized in some domain (e.g., Fourier for convolution), then (4.7) can be implemented very efficiently. For the image separation problem, where $\mathcal{K} = \mathrm{Id}_N$, the update of the component u_s reduces to the convex sum

$$u_s^{(\ell+1)} = (1+\mu)^{-1}(r_s + \mu \hat{u}_s).$$

For the inpainting problem, the update becomes

$$u_s^{(\ell+1)}[i] = \begin{cases} (1+\mu)^{-1}(r_s[i] + \mu \hat{u}_s[i]) & \text{if} \quad i \in \Omega, \\ \hat{u}_s[i] & \text{if} \quad i \notin \Omega. \end{cases}$$

4.5. Step 3: Update of the dictionaries $\{D_s\}_{s\in\Lambda^{\mathrm{L}}}$.

This update step concerns only local learned dictionaries D_s for $s \in \Lambda^{\mathrm{L}}$. Since this problem is separable in each dictionary, this optimization is carried out independently for each D_s. This corresponds to

$$D_s \in \underset{D\in\mathcal{D}_s}{\operatorname{argmin}} \sum_k \|R_k(u_s) - Dx_{s,k}\|^2 = \underset{D\in\mathcal{D}_s}{\operatorname{argmin}} \|U_s - DX_s\|_F^2, \tag{4.9}$$

where $\|.\|_F$ stands for the Frobenius norm, the convex set $\mathcal{D}_s$ is defined in (4.3), $U_s \in \mathbb{R}^{n\times N/\Delta^2}$ is the matrix whose kth column is $R_k(u_s) \in \mathbb{R}^n$, and $X_s \in \mathbb{R}^{m_s\times N/\Delta^2}$ is the matrix whose kth column is $x_{s,k} \in \mathbb{R}^{m_s}$.

The minimization of (4.9) is accomplished by means of a projected gradient descent, which computes iterates $D_s^{(\ell)}$ such that

$$D_s^{(\ell+1)} = \mathcal{P}_{\mathcal{D}_s}\left(D_s^{(\ell)} + \tau(U_s - D_s^{(\ell)}X_s)X_s^*\right), \tag{4.10}$$

where $0 < \tau < 2/\|X_s X_s^*\|$ is the descent step size and

$$(\tilde{d}_j)_{j=0}^{m_s-1} = \mathcal{P}_{\mathcal{D}_s}(D)$$

is the projection of $D = (d_j)_{j=0}^{m_s-1}$ on the convex set $\mathcal{D}_s$, which has an explicit expression

$$\tilde{d}_j = \frac{d_j - c}{\|d_j - c\|} \quad \text{with} \quad c = \frac{1}{n}\sum_{i=0}^{n-1} d_j[i].$$

We note that the linear constraint $\sum_i d_{j,s}[i] = 0$ can be dropped if each patch $R_k(u_s)$, as a column vector in the matrix U_s, is centered by subtracting its mean prior to the dictionary update.

It is worth noting that potentially more efficient schemes, such as Nesterov multistep descent [43, 44] or block-coordinate minimization [33], could be used to solve (4.9). Other approximate methods, potentially faster, have been used to perform the update of the dictionary [23, 1], but they do not minimize (4.9) exactly.

Figure 1 shows two examples of dictionaries learned from input exemplar textures. One can see that the learned atoms d_j do a good job of capturing the patterns of the exemplar texture.

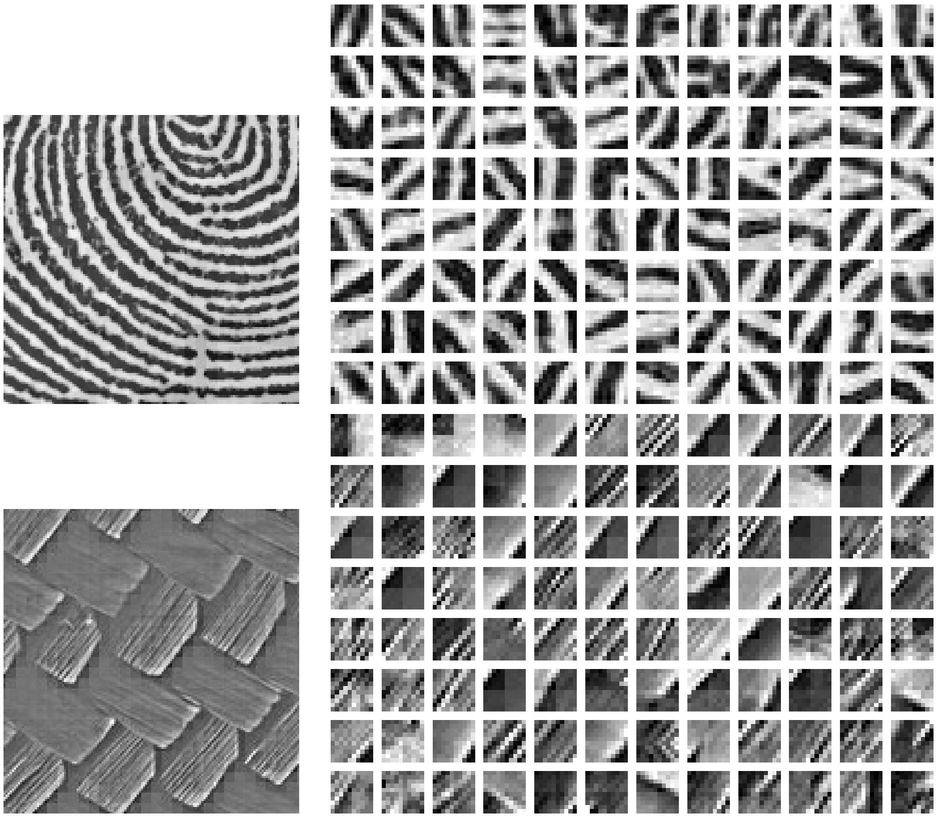

Exemplars $\tilde{u}_1$ and $\tilde{u}_2$ Dictionaries D_1 and D_2

Figure 1. *Examples of dictionary learning on two textures, with patches of size* $\tau \times \tau = 10 \times 10$ *pixels (only a subset of the atoms is displayed on the right).*

4.6. Adaptive MCA algorithm. The adaptive MCA scheme is summarized in Algorithm 1. It iteratively cycles between the above three steps. Each step is carried out using an inner iterative algorithm, with convergence tolerances η_{coef}, η_{comp}, and η_{dico} associated to each of the corresponding inner iteration.

Initialization of the dictionaries. Since the energy $\mathcal{E}$ minimized by the adaptive MCA is nonconvex, different initializations for the dictionaries $\{D_s\}_{s\in\Lambda^{\mathrm{L}}}$ might lead to different solutions. In the numerical experiments detailed in section 5, we consider several initialization scenarios, which may require some user intervention.

Algorithm 1: Adaptive Morphological Component Analysis.

```
Input: observation $f$, fixed dictionaries $\{D_s\}_{s\in\Lambda^{\mathrm{F}}}$, parameters $\mu$ and $\lambda$;
Initialization: $\forall\, s \in \Lambda, u_s = 0$, $\forall\, s \in \Lambda^{\mathrm{L}}$ initialize $D_s$;
while not converged do
    begin Update the coefficients:
        for each $s \in \Lambda^{\mathrm{F}}$ do
            compute $x_s$ by minimizing (4.4) with tolerance $\eta_{\mathrm{coef}}$,
        for each $s \in \Lambda^{\mathrm{L}}$, each $k$ do
            compute $x_{s,k}$ by minimizing (4.5) with tolerance $\eta_{\mathrm{coef}}$.
    end
    begin Update the components: set $\ell = 0$ $\forall\, s \in \Lambda, u_s^{(0)} = u_s$
        repeat
            for each $s \in \Lambda$ do
                compute $u_s^{(\ell+1)}$ using (4.7).
        until $\max_s \|u_s^{(\ell+1)} - u_s^{(\ell)}\| < \eta_{\mathrm{comp}}$;
        Set $\forall\, s, u_s = u_s^{(\ell+1)}$;
    end
    begin Update the dictionaries:
        for each $s \in \Lambda^{\mathrm{L}}$ do set $\ell = 0$, $D_s^{(0)} = D_s$
            repeat
                compute $D_s^{(\ell+1)}$ using (4.10).
            until $\|D_s^{(\ell+1)} - D_s^{(\ell)}\| < \eta_{\mathrm{dico}}$;
            Set $D_s = D_s^{(\ell+1)}$.
    end
Output: Estimated components $\{u_s\}_{s\in\Lambda}$.
```

Convergence of adaptive MCA. The following result ensures that this adaptive MCA algorithm converges to a stationary point of the energy $\mathcal{E}$.

Proposition 4.1. *Suppose that each of steps* 1–3 *is solved exactly by the adaptive MCA algorithm. Then, the obtained sequence of iterates is defined and bounded, and every accumulation point is a stationary point of* $\mathcal{E}$.

Proof. The optimization problem (4.1) has at least one solution by coercivity. The convergence proof of the block-relaxation minimization scheme follows, after identifying our energy in (4.1)–(4.2) with the one considered by Tseng in [59]. Indeed using a notation comparable to that of [59], we can write $\mathcal{E}(\{u_s\}_s, \{x_s\}_s, \{D_s\}_{s\in\Lambda^{\mathrm{L}}})$ as

$$J_0(\{D_s\}_s, \{u_s\}_s, \{x_s\}_s) + J_D(\{D_s\}_{s\in\Lambda^{\mathrm{L}}}) + J_u(\{u_s\}_s) + \sum_s J_x^s(x_s),$$

where

$$J_0(\{D_s\}_s, \{u_s\}_s, \{x_s\}_s) = \frac{\mu}{2} \sum_{s\in\Lambda^{\mathrm{F}}} \|u_s - D_s x_s\|^2 + \frac{\mu}{2p} \sum_{s\in\Lambda^{\mathrm{L}},k} \|R_k(u_s) - D_s x_{s,k}\|^2,$$

$$J_D(\{D_s\}_s) = \begin{cases} 0 & \text{if} \quad D_s \in \mathcal{D}_s \quad \forall s \in \Lambda^{\mathrm{L}}, \\ +\infty & \text{if} \quad D_s \notin \mathcal{D}_s \quad \text{for some } s \in \Lambda^{\mathrm{L}}, \end{cases}$$

$$J_u(\{u_s\}_s) = \frac{1}{2}\left\| f - \mathcal{K}\sum_s u_s \right\|^2,$$

$$J_x^s(x_s) = \begin{cases} \mu\lambda\|x_s\|_1 & \text{(fixed dictionary)} \\ \mu\lambda/p \sum_k \|x_{s,k}\|_1 & \text{(learned dictionary)} \end{cases} \quad \forall s \in \Lambda.$$

It is not difficult to see that J_0 has a nonempty open domain and is continuously differentiable on its domain. Thus J_0 satisfies Assumption A.1 in [59]. Moreover, $\mathcal{E}$ is continuous on its effective domain, with bounded level sets. $\mathcal{E}$ is also convex in $(u_1, \ldots, u_{|\Lambda|}, x_1, \ldots, x_{|\Lambda|})$, and J_D is convex. Thus, Lemma 3.1 and Theorem 4.1(b) of [59] imply that the sequence of iterates provided by the block coordinate descent MCA algorithm is defined and bounded, and every accumulation point is a stationary point of $\mathcal{E}$. ■

It is important to note that the convergence is guaranteed only for an exact adaptive MCA that performs an exact coordinatewise minimization at each of the three steps. Little is known about the behavior of an approximate block coordinate descent, and the tolerances η_{coef}, η_{comp}, and η_{dico} should be decayed through the iterations of the MCA to ensure convergence. For the numerical experiments of section 5, we nevertheless used fixed tolerances, and we always observed empirically the convergence of the algorithm.

Varying threshold. An important feature of the MCA is that the value of the parameter μ is decreased through iterations until it reaches its final value that is adapted to the noise level. This allows one to speed up the convergence and is reminiscent of strategies employed in continuation and path following methods for solving BPDN [18, 46]. Note that more sophisticated threshold update schedules might be used; see, for instance, [8].

Computational complexity. The bulk of computation in step 1 of Algorithm 1 is invested in the application of the matrix D_s and its adjoint D_s^*. For fixed dictionaries corresponding to tight frames used in this paper, these matrices are never explicitly constructed. Rather, they are implemented as fast implicit analysis and synthesis operators. The complexity of these operators for the wavelet D_{wav}, local DCT D_{dct}, and curvelets D_{curv} is $O(N\log(N))$ operations. For learned dictionaries, the matrices $D_s \in \mathbb{R}^{n\times m_s}$ are explicitly constructed, but their size is much smaller than that of fixed dictionaries.

The number of required iterations depends on the tolerance η_{coef} and on the algorithm used for the minimization. Nesterov multistep descent [43, 44] enjoys a fast decay of the ℓ^1-regularized objective with an $O(1/\ell^2)$ rate on the objective. This is much faster than the convergence rate of iterative soft thresholding, which is only $O(1/\ell)$. In practice, the Nesterov multistep scheme performs well.

Each iteration of Step 2 (section 4.4) necessitates reconstructing $\hat{u}_s$ for each s, which can typically be achieved in $O(N)$ or $O(N\log N)$ operations for a fixed dictionary, and in $O(m_s nN/\Delta^2)$ operations for a local learned dictionary. Then the linear system (4.7) must be solved. For separation and inpainting problems, this step is fast and costs at most $O(N)$ for each s. The complexity of each iteration of the projected gradient descent of Step 3 (section 4.5) is similar to the complexity of Step 2.

5. Numerical examples.

Throughout all the numerical examples, we use patches of width $\tau = 10$ pixels for the local learned dictionaries, with an overlap of $\Delta = \tau/2$. For all experiments, we artificially add a Gaussian white noise ε of standard deviation $\sigma/\|f\|_\infty = 0.03$. The parameters λ and μ have been selected as explained in section 4.2.

5.1. Image decomposition.

We recall that the image decomposition problem corresponds to $\mathcal{K} = \mathrm{Id}_N$ in (4.1). One thus looks for an approximate decomposition $f \approx \sum_s u_s$.

Image decomposition with a single adapted layer. We perform two experiments to study the behavior of our algorithm with a fixed dictionary D_1 to capture the sketchy (cartoon) part of the image, and an adapted dictionary D_2 to be learned in order to capture an additional homogeneous texture. When only $|\Lambda^{\mathrm{L}}| = 1$ adapted layer is computed, we find that the obtained results depend only slightly on the initialization. In this case, D_2 is initialized with random patches extracted from the observations f.

Figure 2 (middle row) shows the results of a first separation experiment, where D_1 is a fixed redundant wavelet tight frame and D_2 is a learned dictionary. The adaptive layer is able to capture the fine scale details of the texture. Figure 2 (bottom row) shows the results where D_2 is a fixed local DCT tight frame. This clearly demonstrates that the local DCT is not able to efficiently capture the details of the texture and shows the usefulness and enhancement brought by adaptivity to the separation process.

Figure 3 (top row) displays an example of separation where the layer u_1 has a strong cartoon morphology. We thus use a fixed curvelet dictionary $D_1 = D_{\mathrm{curv}}$. The second layer corresponds to a learned dictionary. Figure 3 (middle row) shows the separation obtained with our adaptive MCA. Although the high pass content of the texture is well captured by the adaptive dictionary, some low pass residual content is visible in the curvelet layer, mainly because elongated curvelet atoms are able to match some patterns of the texture.

We note that in both examples of Figures 2 and 3, the cartoon layer is not perfectly recovered by the adaptive MCA method. In particular, it contains residual oscillations of the original texture layer. This is a consequence of the mutual coherence between the fixed and learned dictionaries. Indeed, both wavelet and curvelet atoms are oscillating and thus capture some of the texture content. The quality of the cartoon layer can be enhanced by adding a total variation penalty as detailed in [55] to direct this component to better fit the piecewise smooth model.

Separation of two textures using exemplars. In this separation scenario, we consider an observed image $f = u_1 + u_2 + \varepsilon$ of $N = 256 \times 256$ pixels, where each u_s corresponds to a stationary texture. We also consider two exemplar textures $(\tilde{u}_1, \tilde{u}_2)$ of 128×128 pixels that are similar to the components to be retrieved. In practice, both u_s and $\tilde{u}_s$ are extracted from the same larger image, at different locations.

The learned dictionaries D_1, D_2 are optimized during the adaptive MCA algorithm, Algorithm 1. They are initialized using the exemplars $(\tilde{u}_1, \tilde{u}_2)$ by minimizing (4.9), where U_s is composed of patches extracted from the exemplars.

Figure 1 shows the two exemplars together with the initialized dictionaries learned from these exemplars. Figure 4 shows the separation obtained with our adaptive MCA, which is of high visual quality because the two textures exhibit a large morphological diversity.

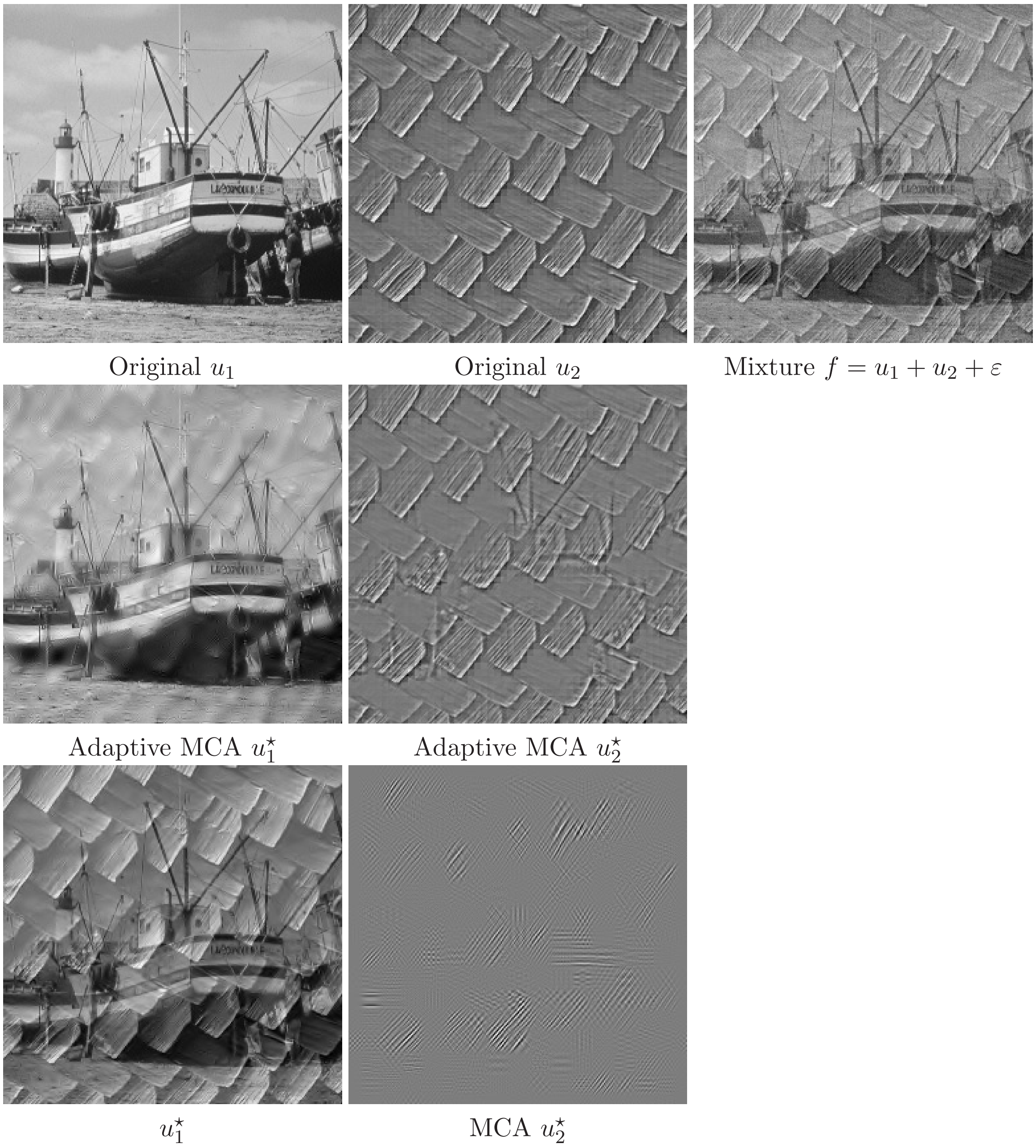

Original u_1 Original u_2 Mixture $f = u_1 + u_2 + \varepsilon$

Adaptive MCA $u_1^\star$ Adaptive MCA $u_2^\star$

$u_1^\star$ MCA $u_2^\star$

Figure 2. *Top row: Original component to be recovered and observed mixture. Middle row: Separation using adaptive MCA with a wavelet dictionary and a learned dictionary. Bottom row: Separation using MCA with a wavelet dictionary and a local DCT dictionary.*

Separation of two textures with user intervention. To study the ability of the adaptive MCA to discriminate between two complicated textures, Figure 5, top, shows a synthetic image obtained by linearly blending two textures $(\tilde{u}_1, \tilde{u}_2)$ as follows:

$$f[i] = \gamma[i]\tilde{u}_1[i] + (1 - \gamma[i])\tilde{u}_2[i] + \varepsilon[i],$$

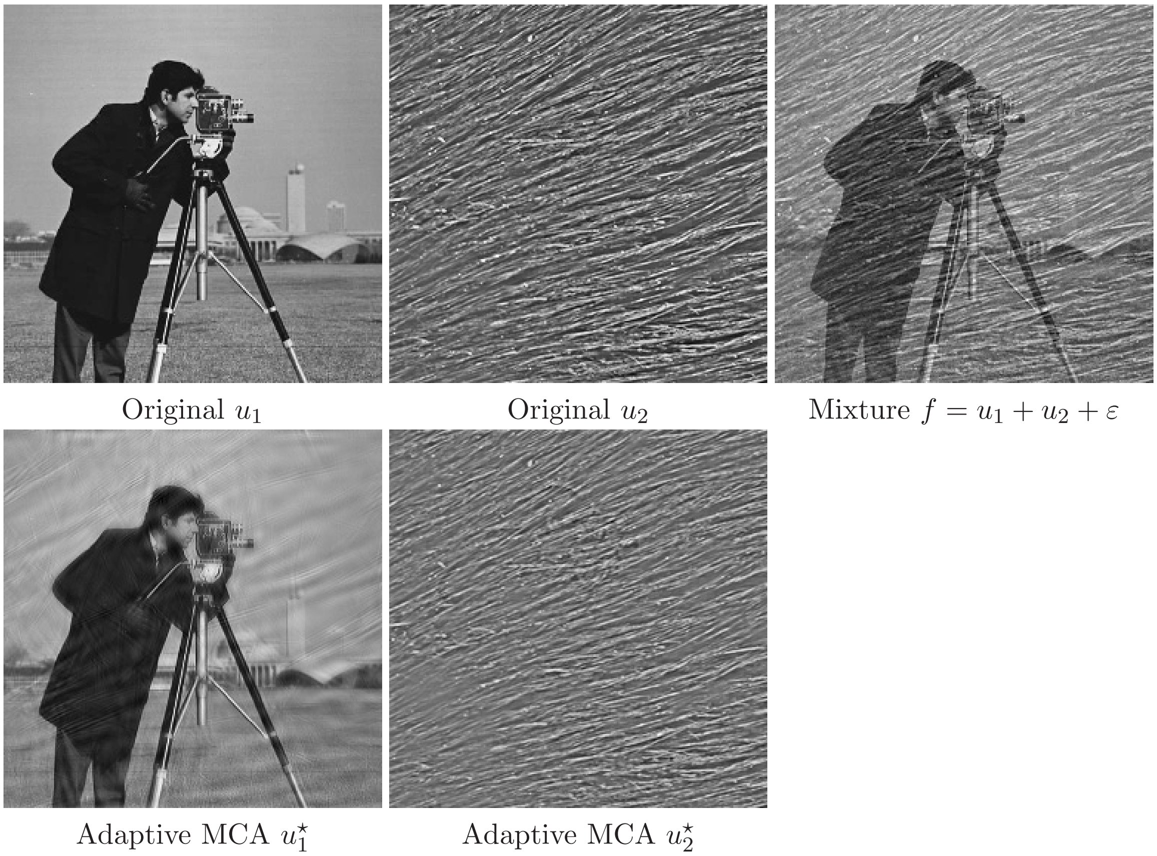

Original u_1 Original u_2 Mixture $f = u_1 + u_2 + \varepsilon$

Adaptive MCA $u_1^\star$ Adaptive MCA $u_2^\star$

Figure 3. *Top row: Original component to be recovered and observed mixture. Bottom row: Separation using adaptive MCA with a curvelet dictionary and a learned dictionary.*

where γ is linearly decaying from 1 to 0 along the horizontal axis.

We use two adapted dictionaries (D_1, D_2) to perform the separation. The user intervention is required to initialize these dictionaries by extracting random patches from the left and the right part, respectively, of the observed image f.

Figures 6 and 7 show the application of the adaptive MCA to natural images, where no ground-truth (oracle) separation result is known. The user intervention is required to give an approximate location of the pattern to extract for each layer u_s.

Discussion about adaptive texture separation. We note that our method does not provide a fully unsupervised texture separation since the user needs to roughly indicate the location where each textural pattern is present. In our approach, the separation process is not penalized if atoms are exchanged wrongfully between different dictionaries, which explains the need for user intervention. A possible extension of our approach might be to include additional constraints $D_s \in \mathcal{D}_s$ beyond imposing zero mean and bounded norm (4.3). For instance, one could force the atoms of a given dictionary to have some frequency localization, anisotropy, or orientation by adding a set of convex constraints. Another extension of our method could integrate interdictionary penalties such as the discriminative learning detailed in [34].

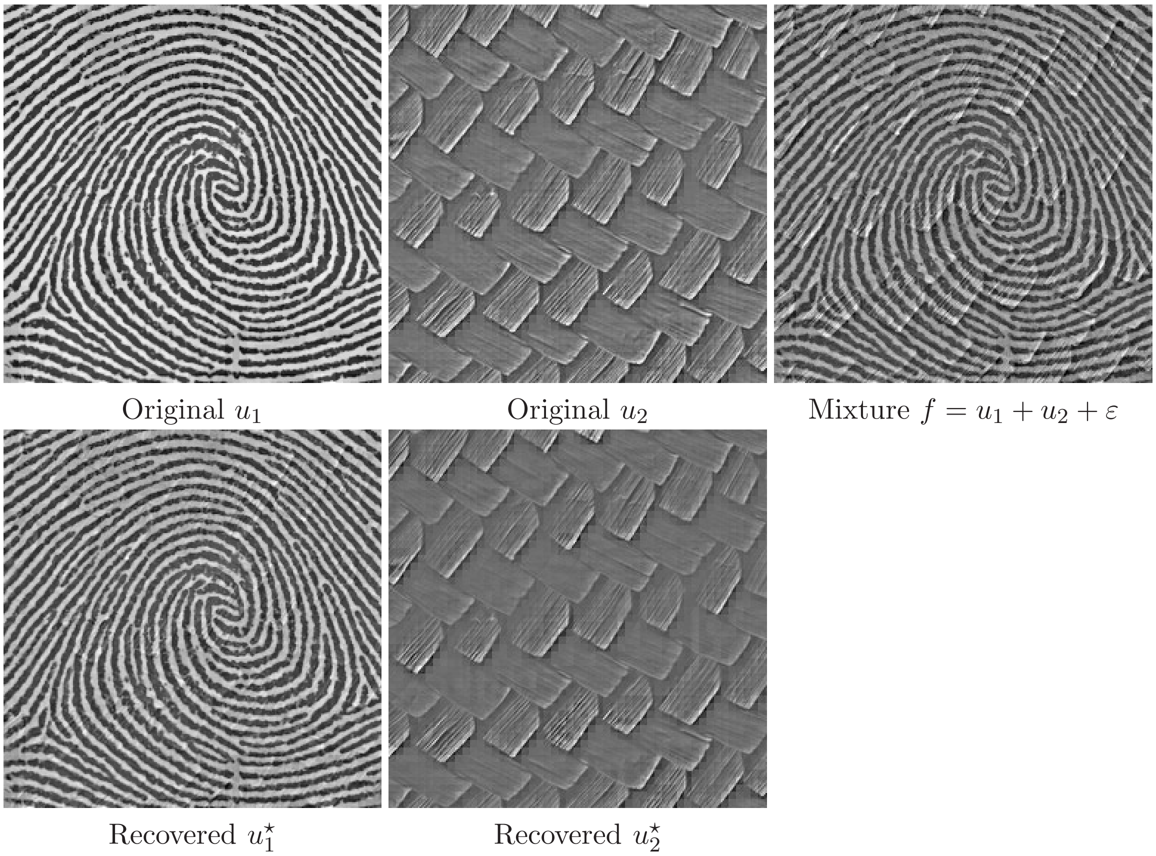

Original u_1

Original u_2

Mixture $f = u_1 + u_2 + \varepsilon$

Recovered $u_1^\star$

Recovered $u_2^\star$

Figure 4. *Example of texture separation using learned dictionaries initialized from exemplars.*

5.2. Inpainting small gaps. Figure 8 depicts an example of inpainting to restore an image $f = \mathcal{K}u + \varepsilon$, where 65% of the pixels are missing. The original image $u = \sum_{s=1}^{3} u_s$ is a superposition of a piecewise smooth cartoon layer, a locally oscillating texture (scarf), and a texture similar to the one in Figure 2. This figure compares the result of inpainting with and without an additional layer corresponding to the learned dictionary D_3, with redundancy $m_3/n = 2$. In both results, the fixed dictionaries D_{wav} and D_{dct} were used. One can see that the inpainting result with a learned dictionary is able to recover the missing fine scale details of the complex texture, which is not the case with the use of a fixed local cosine dictionary D_{dct} alone to represent the texture.

Figure 9 shows another example of inpainting with gaps of medium size. Again, the inpainting with an additional learned dictionary D_3 brings some improvement over the inpainting obtained using standard MCA with only fixed dictionaries, although the improvement is visually less important than with the random mask used in Figure 8. Our method, however, not only solves the inpainting problem, but also yields an intuitive separation of the resulting inpainted image, which might be relevant for some applications. Such applications include object tracking and recognition [58, 56], edge detection after getting rid of texture [55], or textured artifact removal in imaging devices such as those used in astronomy [54].

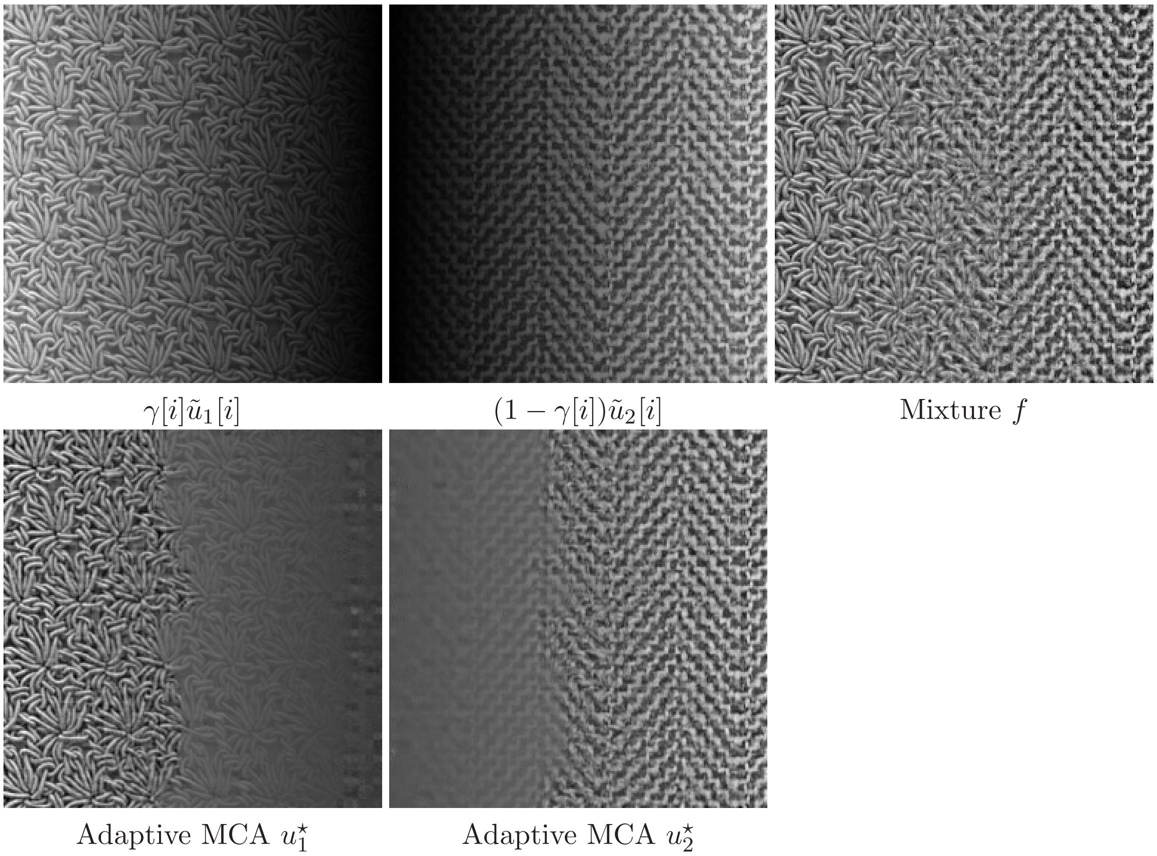

$\gamma[i]\tilde{u}_1[i]$ $(1-\gamma[i])\tilde{u}_2[i]$ Mixture f

Adaptive MCA $u_1^\star$ Adaptive MCA $u_2^\star$

Figure 5. *Example of adaptive separation using two learned dictionaries initialized by the user.*

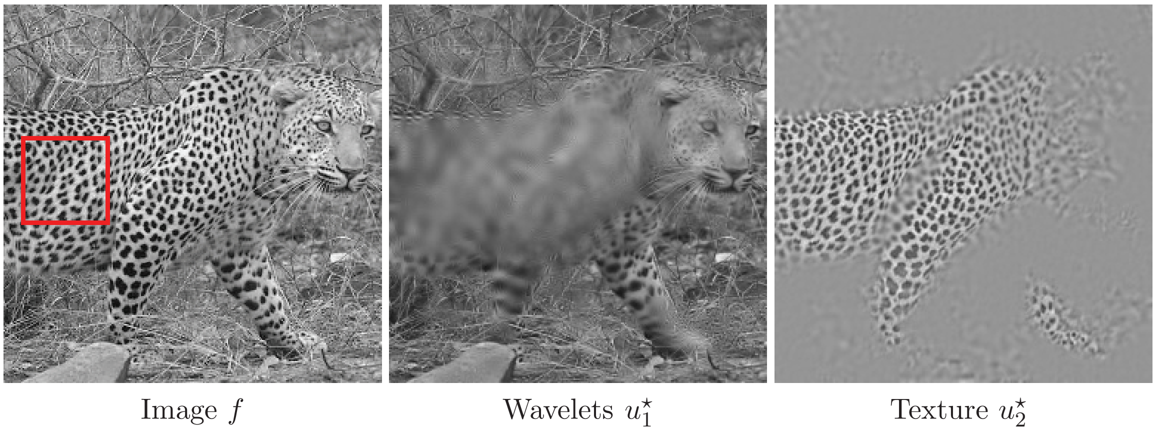

Image f Wavelets $u_1^\star$ Texture $u_2^\star$

Figure 6. *Example of adaptive separation of a natural image into a cartoon layer and a texture layer. The rectangle shows the region given by the user to initialize the dictionary.*

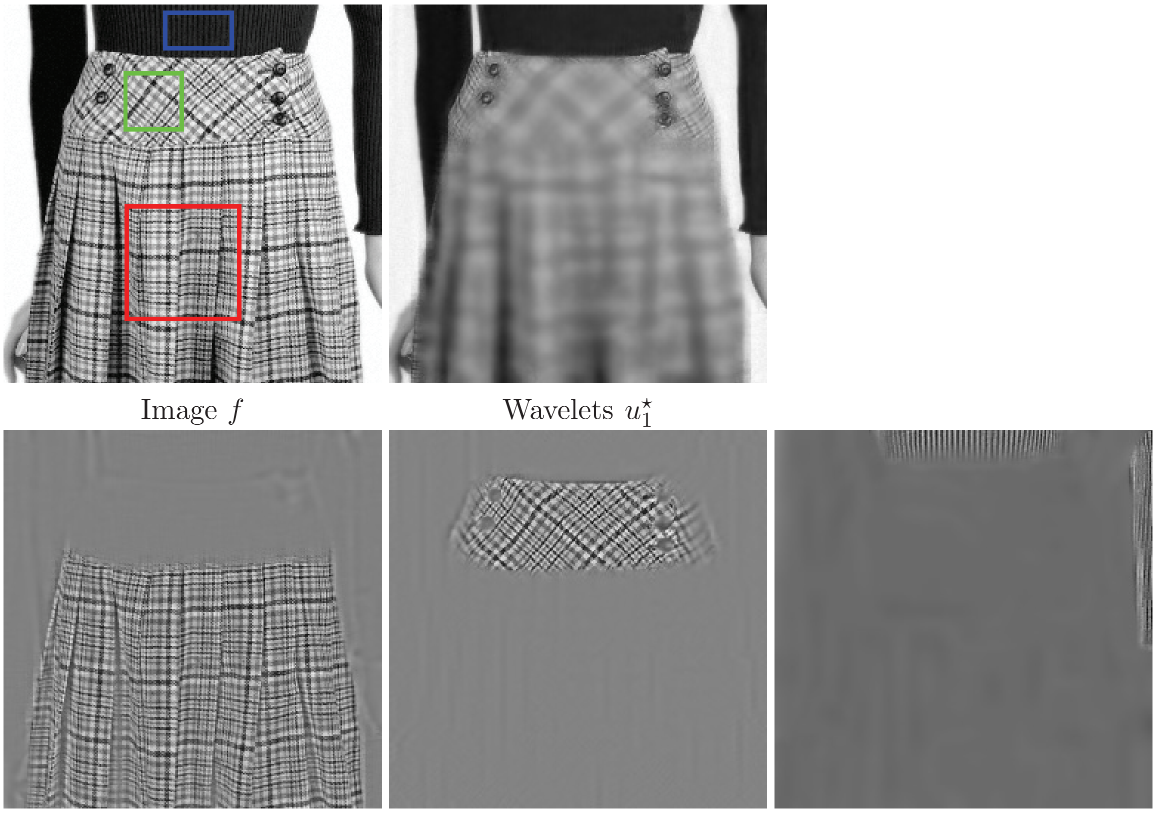

Image f Wavelets $u_1^\star$

Texture $u_2^\star$ Texture $u_3^\star$ Texture $u_4^\star$

Figure 7. *Example of adaptive separation of a natural image into a cartoon layer and three texture layers. The rectangles show the regions given by the user to initialize the dictionaries.*

Discussion about adaptive texture inpainting. We note that, similarly to other dictionary learning approaches [36] and related methods such as fields of experts [51], our approach is restricted to the inpainting of small gaps. The sparsity regularization is indeed efficient if the width of missing regions is smaller that the width τ of the patches. For large gaps, these methods tend to produce a blurry reconstruction in the middle of the missing region. Inpainting large missing regions corresponds to a synthesis problem and should be attacked under the umbrella of other approaches based either on high order PDEs for cartoon inpainting [10, 5, 3] or on patch recopy [19, 13] for more general (texture) pattern inpainting.

Conclusion. We have proposed a new adaptive provably convergent algorithm to perform structure and texture separation using both fixed and learned dictionaries, along with an application to the simultaneous separation and inpainting problem. The main feature of the method is its ability to jointly decompose the image and learn the local dictionaries, which allows one to adapt the process to the properties of the textures to be extracted. Numerical examples have shown that this adaptivity improves the efficiency and visual quality of the separation and inpainting. We have also shown that handling several learned dictionaries is possible, but this requires special care to be taken at the initialization to achieve the desired separation effect.

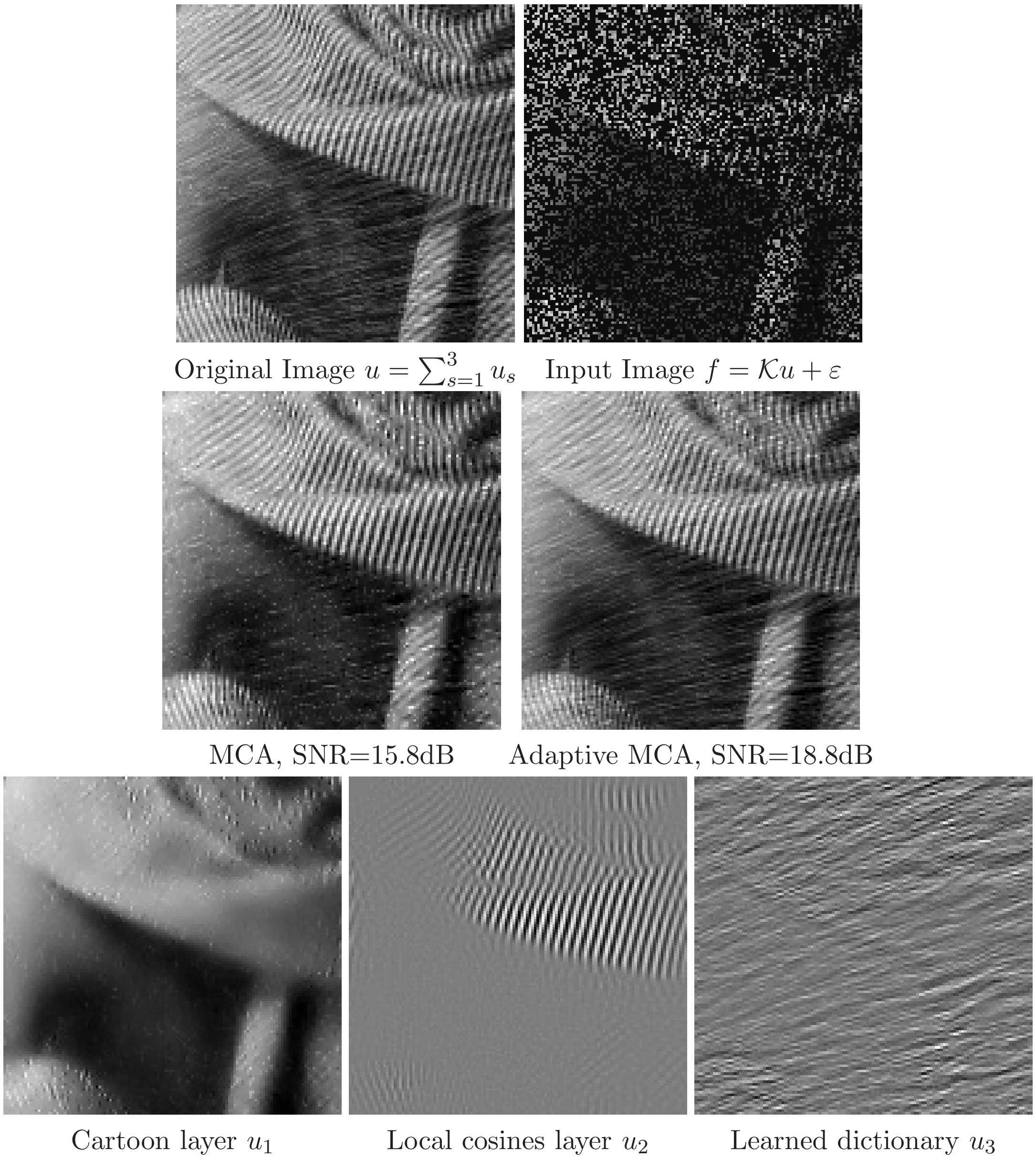

Original Image $u = \sum_{s=1}^{3} u_s$ Input Image $f = \mathcal{K}u + \varepsilon$

MCA, SNR=15.8dB Adaptive MCA, SNR=18.8dB

Cartoon layer u_1 Local cosines layer u_2 Learned dictionary u_3

Figure 8. *Top row: Original image and masked image with 65% randomly removed pixels. Middle row: Inpainted images provided by the standard and adaptive MCA algorithms. Bottom: The three layers provided by the adaptive MCA algorithm.*

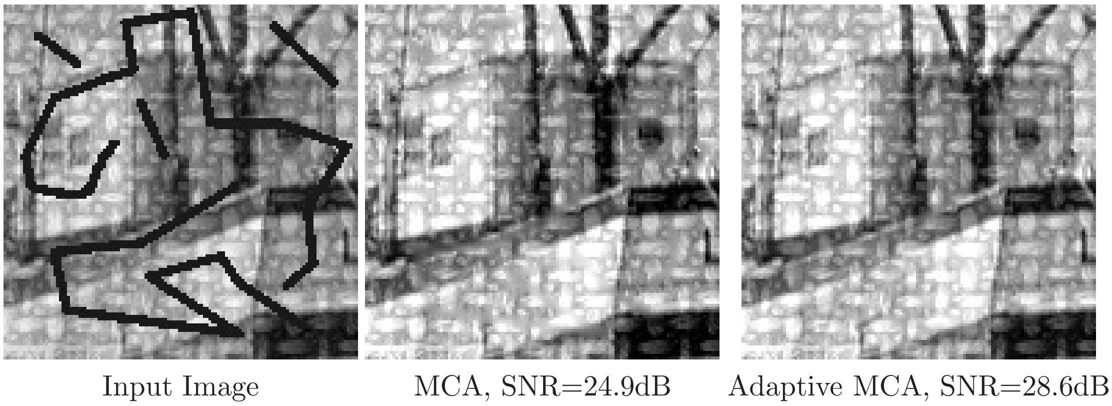

Figure 9. *Image inpainting with a structured mask containing moderately large gaps.*

REFERENCES

[1] M. Aharon, M. Elad, and A. Bruckstein, *The K-SVD: An algorithm for designing of overcomplete dictionaries for sparse representation*, IEEE Trans. Signal Process., 54 (2006), pp. 4311–4322.

[2] J. F. Aujol, G. Aubert, L. Blanc-Feraud, and A. Chambolle, *Image decomposition into a bounded variation component and an oscillating component*, J. Math. Imaging Vision, 22 (2005), pp. 71–88.

[3] C. Ballester, M. Bertalmio, V. Caselles, G. Sapiro, and J. Verdera, *Filling-in by joint interpolation of vector fields and gray levels*, IEEE Trans. Image Process., 10 (2001), pp. 1200–1211.

[4] A. J. Bell and T. J. Sejnowski, *The independent components of natural scenes are edge filters*, Vision Research, 37 (1997), pp. 3327–3338.

[5] M. Bertalmìo, G. Sapiro, V. Caselles, and C. Ballester, *Image inpainting*, in Proceedings of the 27th Annual Conference on Computer Graphics and Interactive Techniques, ACM Press, Addison–Wesley, New York, 2000, pp. 417–424.

[6] J. Bioucas-Dias, *Bayesian wavelet-based image deconvolution: A GEM algorithm exploiting a class of heavy-tailed priors*, IEEE Trans. Image Process., 15 (2006), pp. 937–951.

[7] J. Bobin, J.-L. Starck, J. Fadili, and Y. Moudden, *Sparsity and morphological diversity in blind source separation*, IEEE Trans. Image Process., 16 (2007), pp. 2662–2674.

[8] J. Bobin, J.-L. Starck, J. M. Fadili, Y. Moudden, and D. L. Donoho, *Morphological component analysis: An adaptive thresholding strategy*, IEEE Trans. Image Process., 16 (2007), pp. 2675–2681.

[9] E. Candès and D. Donoho, *New tight frames of curvelets and optimal representations of objects with piecewise C^2 singularities*, Comm. Pure Appl. Math., 57 (2004), pp. 219–266.

[10] V. Caselles, J. M. Morel, and C. Sbert, *An axiomatic approach to image interpolation*, IEEE Trans. Image Process., 7 (1998), pp. 376–386.

[11] S. S. Chen, D. L. Donoho, and M. A. Saunders, *Atomic decomposition by basis pursuit*, SIAM J. Sci. Comput., 20 (1998), pp. 33–61.

[12] P. L. Combettes and V. R. Wajs, *Signal recovery by proximal forward-backward splitting*, Multiscale Model. Simul., 4 (2005), pp. 1168–1200.

[13] A. Criminisi, P. Pérez, and K. Toyama, *Region filling and object removal by exemplar-based image inpainting*, IEEE Trans. Image Process., 13 (2004), pp. 1200–1212.

[14] I. Daubechies, M. Defrise, and C. D. Mol, *An iterative thresholding algorithm for linear inverse problems with a sparsity constraint*, Comm. Pure Appl. Math., 57 (2004), pp. 1413–1541.

[15] L. Demanet and L. Ying, *Wave atoms and sparsity of oscillatory patterns*, Appl. Comput. Harmon. Anal., 23 (2007), pp. 368–387.

[16] D. Donoho, *Wedgelets: Nearly minimax estimation of edges*, Ann. Statist., 27 (1999), pp. 859–897.

[17] D. Donoho and I. Johnstone, *Ideal spatial adaptation via wavelet shrinkage*, Biometrika, 81 (1994), pp. 425–455.

[18] B. Efron, T. Hastie, I. Johnstone, and R. Tibshirani, *Least angle regression*, Ann. Statist., 32 (2004), p. 407–499.

[19] A. A. Efros and T. K. Leung, *Texture synthesis by non-parametric sampling*, in Proceedings of the International Conference on Computer Vision (ICCV '99), Vol. 2, IEEE Computer Society, Washington, DC, 1999, pp. 1033–1038.

[20] M. Elad and M. Aharon, *Image denoising via sparse and redundant representations over learned dictionaries*, IEEE Trans. Image Process., 15 (2006), pp. 3736–3745.

[21] M. Elad, P. Milanfar, and R. Rubinstein, *Analysis versus synthesis in signal priors*, Inverse Problems, 23 (2007), pp. 947–968.

[22] M. Elad, J.-L. Starck, D. Donoho, and P. Querre, *Simultaneous cartoon and texture image inpainting using morphological component analysis (MCA)*, Appl. Comput. Harmon. Anal., 19 (2005), pp. 340–358.

[23] K. Engan, S. O. Aase, and J. H. Husoy, *Method of optimal directions for frame design*, in Proceedings of the 1999 IEEE International Conference on Acoustics, Speech, and Signal Processing (ICASSP '99), IEEE Computer Society, Washington, DC, 1999, pp. 2443–2446.

[24] M. J. Fadili and J.-L. Starck, *Sparse representation-based image deconvolution by iterative thresholding*, in Proceedings of the Astronomical Data Analysis Conference IV, F. Murtagh and J.-L. Starck, eds., Marseille, France, CEA Saclay, Gif-sur-Yvette, France, 2006.

[25] M. J. Fadili, J.-L. Starck, and F. Murtagh, *Inpainting and zooming using sparse representations*, Computer J., 52 (2007), pp. 64–79.

[26] M. Figueiredo and R. Nowak, *An EM algorithm for wavelet-based image restoration*, IEEE Trans. Image Process., 12 (2003), pp. 906–916.

[27] M. Figueiredo and R. Nowak, *A bound optimization approach to wavelet-based image deconvolution*, in Proceedings of the IEEE International Conference on Image Processing (ICIP), 2005, pp. 782–785.

[28] K. Kreutz-Delgado, J. F. Murray, B. D. Rao, K. Engan, T.-W. Lee, and T. Sejnowski, *Dictionary learning algorithms for sparse representation*, Neural Comput., 15 (2003), pp. 349–396.

[29] E. Le Pennec and S. Mallat, *Bandelet image approximation and compression*, Multiscale Model. Simul., 4 (2005), pp. 992–1039.

[30] S. Lesage, R. Gribonval, F. Bimbot, and L. Benaroya, *Learning unions of orthonormal bases with thresholded singular value decomposition*, in Proceedings of the IEEE International Conference on Acoustics, Speech, and Signal Processing (ICASSP), 2005, pp. 293–296.

[31] M. S. Lewicki and T. J. Sejnowski, *Learning overcomplete representations*, Neural Comput., 12 (2000), pp. 337–365.

[32] L. Lieu and L. Vese, *Image restoration and decomposition via bounded total variation and negative Hilbert-Sobolev spaces*, Appl. Math. Optim., 58 (2008), pp. 167–193.

[33] J. Mairal, F. Bach, J. Ponce, and G. Sapiro, *Online learning for matrix factorization and sparse coding*, J. Machine Learning Res., 11 (2010), pp. 19–60.

[34] J. Mairal, F. Bach, J. Ponce, G. Sapiro, and A. Zisserman, *Discriminative learned dictionaries for local image analysis*, in Proceedings of the IEEE Conference on Computer Vision and Pattern Recognition, 2008, pp. 1–8.

[35] J. Mairal, F. Bach, J. Ponce, G. Sapiro, and A. Zisserman, *Supervised dictionary learning*, in Advances in Neural Information Processing Systems 21 (Vancouver, Canada, 2008), D. Koller, D. Schuurmans, Y. Bengio, and L. Bottou, eds., MIT Press, Cambridge, MA, 2009, pp. 1033–1040.

[36] J. Mairal, M. Elad, and G. Sapiro, *Sparse representation for color image restoration*, IEEE Trans. Image Process., 17 (2008), pp. 53–69.

[37] S. Mallat, *A Wavelet Tour of Signal Processing*, Academic Press, San Diego, 1998.

[38] S. Mallat, *Geometrical grouplets*, Appl. Comput. Harmon. Anal., 26 (2009), pp. 161–180.

[39] S. Mallat and G. Peyré, *Orthogonal bandlet bases for geometric images approximation*, Comm. Pure Appl. Math., 61 (2008), pp. 1173–1212.

[40] S. Masnou, *Disocclusion: A variational approach using level lines*, IEEE Trans. Image Process., 11 (2002), pp. 68–76.

[41] F. G. Meyer and R. R. Coifman, *Brushlets: A tool for directional image analysis and image compression*, Appl. Comput. Harmon. Anal., 5 (1997), pp. 147–187.

[42] Y. Meyer, *Oscillating Patterns in Image Processing and Nonlinear Evolution Equations*, American Mathematical Society, Boston, 2001.

[43] Yu. Nesterov, *Smooth minimization of non-smooth functions*, Math. Program., 103 (2005), pp. 127–152.

[44] Yu. Nesterov, *Gradient Methods for Minimizing Composite Objective Function*, CORE Discussion Papers 2007/76, Center for Operations Research and Econometrics (CORE), Université catholique de Louvain, Louvain-la-Neuve, Belgium, 2007.

[45] B. A. Olshausen and D. J. Field, *Emergence of simple-cell receptive-field properties by learning a sparse code for natural images*, Nature, 381 (1996), pp. 607–609.

[46] M. R. Osborne, B. Presnell, and B. A. Turlach, *A new approach to variable selection in least squares problems*, IMA J. Numer. Anal., 20 (2000), pp. 389–403.

[47] A. Ozerov and C. Févotte, *Multichannel nonnegative matrix factorization in convolutive mixtures for audio source separation*, IEEE Trans. Audio, Speech, and Language Processing, 18 (2010), pp. 550–563.

[48] G. Peyré, *Sparse modeling of textures*, J. Math. Imaging Vision, 34 (2009), pp. 17–31.

[49] G. Peyré, *Texture processing with grouplets*, IEEE Trans. Pattern Anal. Mach. Intell., 32 (2009), pp. 733–746.

[50] G. Peyré, J. Fadili, and J. Starck, *Learning dictionaries for geometry and texture separation*, in Proceedings of SPIE, Wavelets XII, SPIE, Bellingham, WA, 2007.

[51] S. Roth and M. J. Black, *Fields of experts*, Int. J. Comput. Vision, 82 (2009), pp. 205–229.

[52] L. I. Rudin, S. Osher, and E. Fatemi, *Nonlinear total variation based noise removal algorithms*, Phys. D, 60 (1992), pp. 259–268.

[53] N. Shoham and M. Elad, *Algorithms for signal separation exploiting sparse representations, with application to texture image separation*, in Proceedings of the IEEE 25th Convention of Electrical and Electronics Engineers in Israel, IEEE Computer Society, Washington, DC, 2008, pp. 538–542.

[54] J.-L. Starck, M. Elad, and D. Donoho, *Redundant multiscale transforms and their application for morphological component analysis*, Adv. Imag. Electron Phys., 132 (2004), pp. 287–348.

[55] J.-L. Starck, M. Elad, and D. Donoho, *Image decomposition via the combination of sparse representation and a variational approach*, IEEE Trans. Image Process., 14 (2005), pp. 1570–1582.

[56] D. Tschumperlé, Y. Bentolila, J. Martinot, and M. Fadili, *Fast time-space tracking of smoothly moving fine structures in image sequences*, in Proceedings of the IEEE International Conference on Imaging (ICIP), San Antonio, TX, 2007, 317–320.

[57] D. Tschumperlé and R. Deriche, *Vector-valued image regularization with PDEs: A common framework for different applications*, IEEE Trans. Pattern Anal. Mach. Intell., 27 (2005), pp. 506–517.

[58] D. Tschumperlé, J. Fadili, and Y. Bentolila, *Wire structure pattern extraction and tracking from X-ray images of composite mechanisms*, in Proceedings of the 2006 IEEE Computer Society Conference on Computer Vision and Pattern Recognition (CVPR'06), New York, 2006, pp. 2461–2466.

[59] P. Tseng, *Convergence of a block coordinate descent method for nondifferentiable minimization*, J. Optim. Theory Appl., 109 (2001), pp. 475–494.

[60] L. Vese and S. Osher, *Modeling textures with total variation minimization and oscillating patterns in image processing*, J. Sci. Comput., 19 (2003), pp. 553–572.

[61] M. Zibulevsky and B. A. Pearlmutter, *Blind source separation by sparse decomposition in a signal dictionary*, Neural Comput., 13 (2001), pp. 863–882.